PHYSICAL REVIEW C **82**, 031304(R) (2010)

Rotation alignment in neutron-rich Cr isotopes: A probe of deformed single-particle levels across $N = 40$

Yingchun Yang (杨迎春),[1] Yang Sun (孙扬),[1,2,3,*] Kazunari Kaneko (金子和也),[4] and Munetake Hasegawa (长谷川宗武)[1,2]

[1]*Department of Physics, Shanghai Jiao Tong University, Shanghai 200240, People's Republic of China*

[2]*Institute of Modern Physics, Chinese Academy of Sciences, Lanzhou 730000, People's Republic of China*

[3]*Department of Physics and Astronomy, University of Tennessee, Knoxville, Tennessee 37996, USA*

[4]*Department of Physics, Kyushu Sangyo University, Fukuoka 813-8503, Japan*

(Received 28 July 2010; published 30 September 2010)

Recent experiments have reached the neutron-rich Cr isotope with $N = 40$ and confirmed enhanced collectivity near this subshell. The current data focus on low-spin spectroscopy only, with little information on the states where high-j particles align their spins with the system rotation. By applying the projected shell model, we show that rotation alignment occurs in neutron-rich even-even Cr nuclei as early as spin $8\hbar$ and, owing to shell filling, the aligning particles differ in different isotopes. It is suggested that observation of irregularities in moments of inertia is a direct probe of the deformed single-particle scheme in this exotic mass region.

DOI: 10.1103/PhysRevC.82.031304 PACS number(s): 21.10.Pc, 21.10.Re, 27.40.+z, 27.50.+e

Current nuclear structure studies are devoted to the discussion of enhanced collectivity in the neutron-rich pf-shell nuclei with neutron number $N \approx 40$. One has found strong evidence for compressed first 2^+ energy levels and large E2 transitions linking these and the ground states for several isotopic chains around the proton magic number $Z = 28$, for example, in the Cr ($Z = 24$) [1,2], Fe ($Z = 26$) [3–5], and Zn ($Z = 30$) [6] isotopes. These data support the early suggestions that near $N = 40$, pronounced collectivity develops, corresponding to the formation of a region of deformation [7–9].

In the study of neutron-rich nuclei, an important issue is to understand emerging subshell gaps, which cause substantial modifications of the intrinsic shell structure in nuclei with a neutron excess [10]. While information on collective excitations in low-spin states is useful, comprehensive knowledge of these exotic nuclei requires the study of higher-spin states in which, owing to rotation alignment, quasiparticle (qp) configurations are dominant. For an yrast band consisting of the lowest states for each angular momentum, the aligning particles carry valuable information on the deformed single-particle states. Therefore, investigations of high-spin spectra can yield knowledge of the intrinsic shell structure of single-particle levels.

Microscopic calculations have shown that beginning at $N \approx 30$, energy minima with sizable prolate deformations appear for the neutron-rich Cr isotopes [11]. In these deformed Cr isotopes, protons occupy up to the $\pi f_{7/2}$ orbit, while neutrons of the $N > 28$ isotopes fill in the rest of the pf shell. With the splitting of single-particle orbits owing to deformation, the proton Fermi level lies between the $f_{7/2}$ orbitals $\pi[321]3/2^-$ and $\pi[312]5/2^-$ and, also, is not far from $\pi[300]1/2^-$. In contrast, the down-sloping levels of the neutron intruder $g_{9/2}$ orbit, $\nu[440]1/2^+$, $\nu[431]3/2^+$, and $\nu[422]5/2^+$, are found near the neutron Fermi levels, and therefore, neutrons can easily occupy these orbitals. Thus when nuclei rotate, these high-j particles (here, $f_{7/2}$ for protons and $g_{9/2}$ for neutrons) are among the first to align their rotation with the rotation axis of the system, resulting in observable effects in the moment of inertia (MoI), which correspond to the phenomenon known as rotation alignment [12]. Thus with increasing neutron number from $N = 30$ to $N = 40$ and beyond, these high-j orbits dominate the high-spin behavior of these nuclei. This qualitative picture is also valid for nuclei with a soft ground state. Angular-momentum-projected energy-surface calculations show [13] that as soon as the nuclei begin to rotate, well-defined shapes in favor of prolate deformation develop.

With the experimental advances, detailed spectroscopic measurements of neutron-rich nuclei now become possible. In a very recent work, Gade *et al.* [1] reported their successful experiment on the neutron-rich isotope ^{64}Cr by ^{9}Be-induced inelastic scattering, obtaining the first spectroscopy at the $N = 40$ subshell for Cr isotopes. Data for some lighter Cr isotopes are presently available [2,14,15]. In the near-future, fragmentation of a ^{76}Ge beam may push the experiment to more neutron-rich regions [16]. On the theoretical side, large-scale shell-model calculations [17–19] have been successful in describing the low-spin spectroscopy of neutron-rich nuclei. For example, the spherical shell-model calculation for Cr isotopes [19] including the $g_{9/2}$ orbit in the model space predicted the first excited 4^+ energy of ^{62}Cr, which was later confirmed by experiment [2]. There have been encouraging applications of beyond-mean-field approaches [11,20], which can easily handle a large model space. Nevertheless, models that either do not allow a sufficient number of valence particles in the spherical shell-model space or do not build excited qp configurations in the deformed models may not be appropriate for discussions of high-spin physics.

To discuss high-spin states and to further study the deformed single-particle structure in neutron-rich nuclei, we performed projected shell-model (PSM) [21] calculations for neutron-rich, even-even Cr isotopes with neutron number from 30 to 44 aiming at making predictions ahead of experiment. The model was recently applied to the

*Corresponding author: sunyang@sjtu.edu.cn

TABLE I. Input deformation parameters (ϵ_2) used in the calculation.

	Cr							
	54	56	58	60	62	64	66	68
ε_2	0.210	0.210	0.220	0.240	0.250	0.235	0.235	0.230

neutron-rich Fe isotopes [13], where large 2^+ state B(E2)'s were predicted for ^{62,64}Fe and confirmed later by measurement [5]. It has also been employed to study the yrast structure of Ge nuclei [22]. The PSM calculation uses deformed Nilsson single-particle states [23] to build the model basis. For the present calculations, the quadrupole deformation parameters for building the deformed bases are listed in Table I. These parameters are consistent with the known experimental trend of increasing deformation toward $N = 40$ [15] and, then, a slightly decreasing collectivity as predicted by spherical shell-model calculations [19]. Pairing correlations are incorporated into the Nilsson states by a BCS calculation. The consequence of the Nilsson-BCS calculations defines a set of qp states corresponding to the qp vacuum $|0\rangle$. The PSM wave function is a superposition of (angular-momentum) projected multi-qp states that span the shell-model space:

$$\left|\Psi^{\sigma}_{IM}\right\rangle = \sum_{K\kappa} f^{\sigma}_{IK_\kappa}\, \hat{P}^{I}_{MK} |\Phi_\kappa\rangle, \tag{1}$$

where $|\Phi_\kappa\rangle$ denotes the qp basis, κ labels the basis states, and $f^{\sigma}_{IK_\kappa}$ are determined by the configuration mixing implemented by diagonalization. $\hat{P}^{I}_{MK}$ is the angular momentum projection operator [21] that projects an intrinsic configuration onto states with a good angular momentum. As the valence space for this mass region, particles in three major shells ($N = 2, 3, 4$ for both neutrons and protons) are activated. The multi-qp configurations, consisting of zero-, two-, and four-qp states, for even-even nuclei are as follows:

$$\{|0\rangle, a^{\dagger}_{\nu_i} a^{\dagger}_{\nu_j} |0\rangle\,, a^{\dagger}_{\pi_i} a^{\dagger}_{\pi_j} |0\rangle\,, a^{\dagger}_{\nu_i} a^{\dagger}_{\nu_j} a^{\dagger}_{\pi_k} a^{\dagger}_{\pi_l} |0\rangle\}, \tag{2}$$

where $a^{\dagger}_{\nu}$ and $a^{\dagger}_{\pi}$ are the neutron and proton qp creation operators, respectively, with the subscripts i, j, k, and l denoting the Nilsson quantum numbers that run over the orbitals close to the Fermi levels.

The PSM calculation employs a quadrupole plus pairing Hamiltonian, with inclusion of the quadrupole-pairing term

$$\hat{H} = \hat{H}_0 - \frac{1}{2}\chi \sum_{\mu} \hat{Q}^{\dagger}_{\mu} \hat{Q}_{\mu} - G_M \hat{P}^{\dagger} \hat{P} - G_Q \sum_{\mu} \hat{P}^{\dagger}_{\mu} \hat{P}_{\mu}. \tag{3}$$

In Eq. (3), $\hat{H}_0$ is the spherical single-particle Hamiltonian, which contains a proper spin-orbit force. The monopole pairing strengths are taken to be $G_M = [G_1 \mp G_2(N - Z)/A]/A$, where the plus sign and the minus sign are for protons and neutrons, respectively, with $G_1 = 18.72$ and $G_2 = 10.74$. The quadrupole pairing strength G_Q is assumed to be proportional to G_M, the proportionality constant being fixed to 0.30.

The MoI is a characteristic quantity for the description of rotational behavior. In Fig. 1, the calculated results (filled squares) for the yrast bands in $^{54-68}$Cr are presented in terms of the MoI (defined as $\mathscr{J}(I) = (2I - 1)/[E(I) - E(I - 2)]$) and compared with the available data (filled circles). It is observed that for these isotopes, $\mathscr{J}$ increases nearly linearly with spin I for the lowest spin states. However, irregularities in MoI are seen as early as $I = 8$, with the actual pattern differing in different isotopes. Interestingly, all the current data, with the last one or two data points assigned as tentative in several isotopes, stop at the spins where irregularities are predicted to occur. As we shall discuss, these irregularities reflect changes in the yrast structure caused by rotation alignment of nucleons from specific orbitals. Thus by studying the changes in MoI one can gain valuable information on deformed single-particle states for this exotic mass region.

By examining the MoI patterns in Fig. 1, one finds that with increasing spin, the $\mathscr{J}$ value of the two lightest isotopes, ^{54,56}Cr, either bends down or stops rising at spins $I = 10$ and 12 and then shows a rapid rise. A peak is predicted to occur at $I = 16$ for both isotopes. Irregularities in $\mathscr{J}$ are especially notable in ^{58,60,62}Cr, in which the rotational patterns

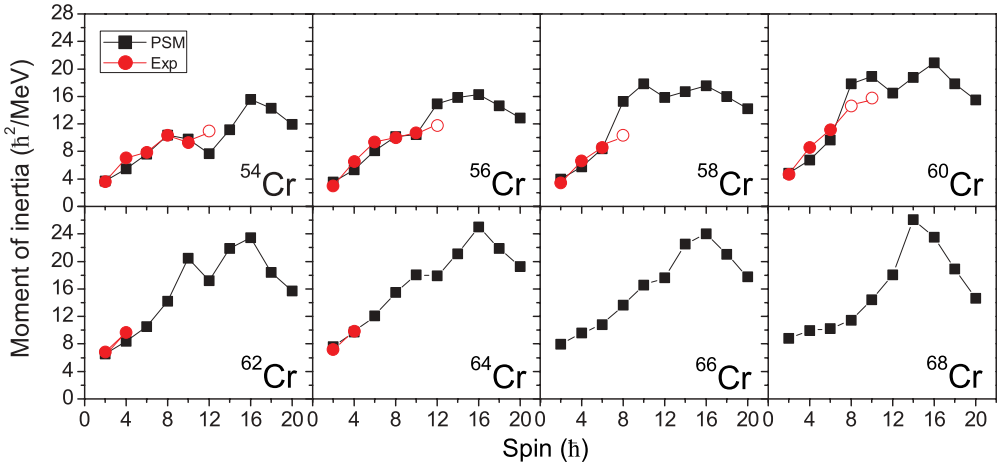

FIG. 1. (Color online) Comparison of the calculated moments of inertia (filled squares) for yrast bands in even-even $^{54-68}$Cr with the known experimental data (filled circles) taken from Ref. [14] for ^{54}Cr, Ref. [15] for $^{56-60}$Cr, Ref. [2] for ^{62}Cr, and Ref. [1] for ^{64}Cr. Open circles denote the tentative data reported in these publications.

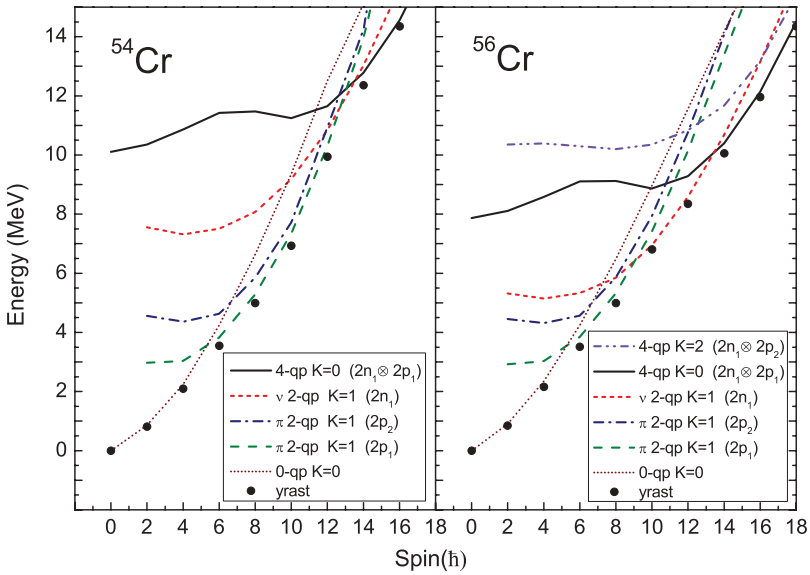

FIG. 2. (Color online) Theoretical band diagrams for ^{54,56}Cr. Bands for some important configurations are shown here and explained in Table II. Note that, to illustrate them clearly, only even-spin states are plotted, to avoid a strong zigzag in curves between even- and odd-spin states.

are interrupted several times. The first one is seen soon after $I = 6$, where a jump in $\mathcal{J}$ is predicted. Later, at $I = 10$ and 16, two peaks are predicted to appear. For the $N \geqslant 40$ isotopes ^{64,66,68}Cr, our calculation suggests a gradual increase in $\mathcal{J}$ (with some small perturbations) up to high spins, until a peak is formed at $I = 14$ or 16.

To understand what causes the variations in MoI, we study theoretical band diagrams for these isotopes. In the PSM, an ensemble of projected configurations plotted in one figure is called a band diagram [21], in which the rotational behavior of each configuration, as well as its relative energy compared to other configurations, is easily visualized. Because our deformed basis states retain axial symmetry, we use K (the projection of angular momentum on the symmetry axis of the deformed body) to classify the configurations. For even-even nuclei, the zero-qp ground band has $K = 0$, whereas a multi-qp band has a K given by the sum of the Nilsson K quantum numbers of its constituent qp's. A superposition of them imposed by configuration mixing gives the final results, with the lowest one at each spin being the yrast state. Study of band crossings in the yrast region can provide useful messages from which to identify the most important configurations for the yrast states.

According to the nature of band crossings, we may divide the isotopes into three groups for discussion. In Figs. 2–4, we plot the important configurations that are used to discuss the MoI variations in Fig. 1. The figures show that as a nucleus starts rotating, the zero-qp ground-band energy increases and the band quickly enters the high-energy region. The two- and four-qp bands rise slowly at low spins and, therefore, can cross the zero-qp band. To facilitate the discussion, we term the relevant two-qp configurations $2n_1$, $2n_2$, $2n_3$, $2p_1$, and $2p_2$, with the details listed in Table II. In the band diagrams, we use different line styles to distinguish different qp bands, so that one

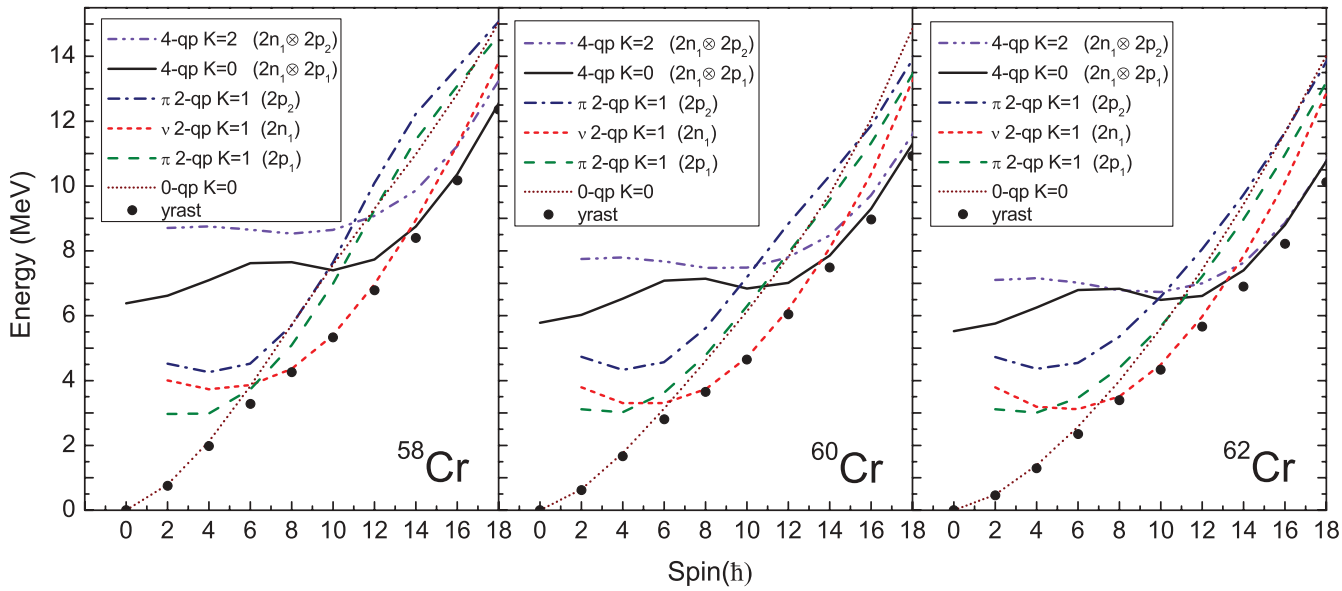

FIG. 3. (Color online) Same as Fig 2, but for ^{58,60,62}Cr.

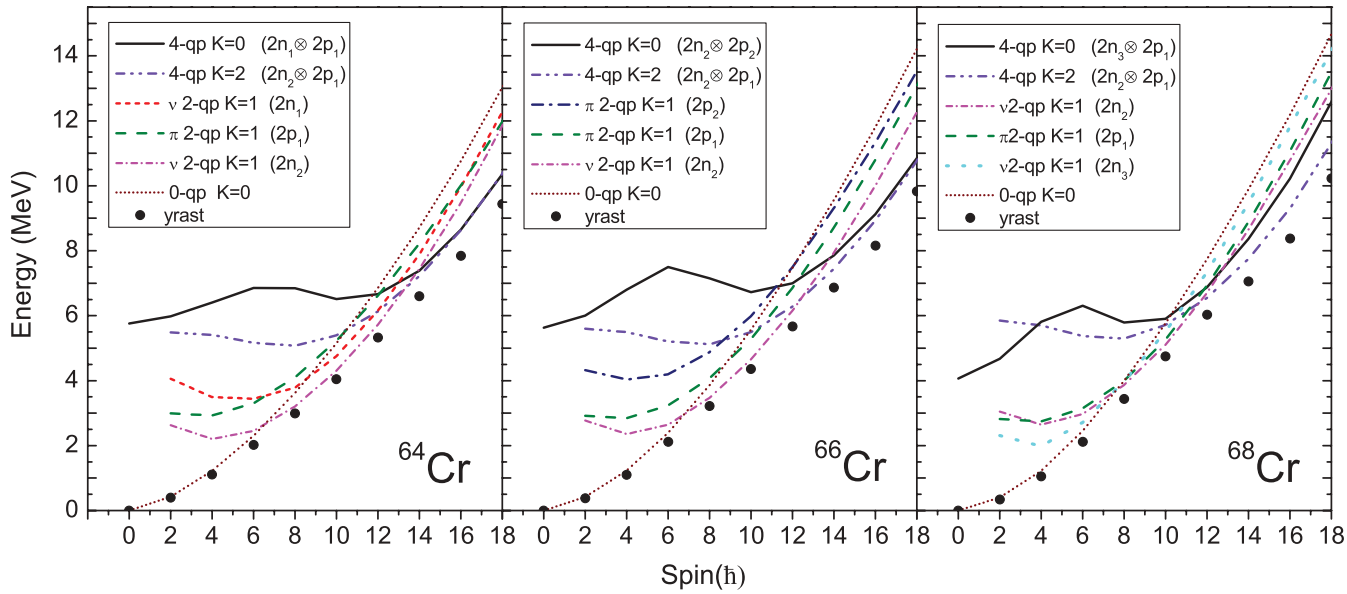

FIG. 4. (Color online) Same as Fig 2, but for ^{64,66,68}Cr.

can easily follow them with increasing neutron number. In addition, the filled circles labeled "yrast" in Figs. 2–4 are the lowest state at each spin obtained after diagonalization, and these are the theoretical results compared with the data (see Fig. 1).

In the two lightest isotopes, ^{54,56}Cr, the neutron $g_{9/2}$ orbitals are far above the Fermi level, and therefore, neutron two-qp states are high in energy. Proton two-qp states are expected to be the first to cross the zero-qp band. Figure 2 indeed shows that the proton two-qp band (labeled $2p_1$) is the lowest two-qp band, which crosses the ground band at $I = 6$. The crossing is gentle so that it causes little disturbance in MoI. Another proton two-qp band (labeled $2p_2$) exhibits a similar character and approaches the $2p_1$ band near $I = 10$. After this spin, the two proton two-qp bands stay nearly parallel and interact with each other. The interaction causes the first irregularity in the MoI of ^{54}Cr at $I \approx 10$, as shown in Fig. 1. The neutron two-qp band $2n_1$ lies high in energy at low spins; however, it crosses the proton two-qp bands at $I \approx 10$ in ^{56}Cr. In the spin interval $I = 12$–14, the four-qp band consisting of two two-qp states, $2n_1$ and $2p_1$, sharply crosses the two-qp bands. After $I \approx 14$, the yrast states are predicted to be of a four-qp structure. The four-qp band crossing changes the content of the yrast wave functions, leading to the second irregularity in MoI of ^{54,56}Cr, as shown in Fig. 1.

Going toward $N = 40$, very irregular MoI values are predicted in Fig. 1 for ^{58,60,62}Cr. This is because as neutrons begin to fill the $g_{9/2}$ shell, the low-K orbitals come close to the Fermi level. It is known that for nucleons of low-K, high-j orbitals, it is easy to align the spins with the rotation. Figure 3 shows that although the lowest two-qp band at low spins, $I < 6$, is the proton $2p_1$, it climbs rapidly and soon becomes unimportant. The other proton two-qp band beginning at a higher energy shows a similar character. In contrast, the neutron two-qp band (labeled $2n_1$), which is coupled by two neutrons in the low-K $g_{9/2}$ orbitals, is more important because it crosses the ground band at $I = 6$ and dominates the yrast structure in the spin interval $I = 6$–14. The crossing leads to a jump in MoI predicted at $I = 6$ or 8, as shown in Fig. 1. The prediction is at variance with the current tentative data [15], which seem to suggest a more regular rise in MoI. There are two four-qp bands in each isotope shown in Fig. 3, among which the $K = 0$ four-qp band is more notable, as it crosses the neutron two-qp band $2n_1$ at spin $I \approx 14$ and becomes yrast after that spin. The peak in MoI at $I \approx 16$ in ^{58,60,62}Cr is attributed to the crossing of the four-qp band.

Band diagrams for the heavier isotopes, ^{64,66,68}Cr, are plotted in Fig. 4. With increasing neutron number, the $2n_1$ configuration lies far from the Fermi level. Instead, the other two neutron two-qp bands, $2n_2$ and $2n_3$, play a role. Because in the $2n_2$ and $2n_3$ configurations there are higher-K states that are more coupled, the rotational behavior of $2n_2$ and $2n_3$ is different from $2n_1$. The two-qp bands with high-K states exhibit rotational behavior similar to that of the ground band, and therefore, crossing of them is always gentle. This makes an observable difference in MoI: although $2n_2$ and $2n_3$ bands cross the ground band at $I \approx 6$, no notable variation in MoI can be seen in Fig. 1. The yrast states of high spins ($I > 14$) are predicted to be strongly mixed by the $K = 2$ four-qp configuration. Peaks in MoI at high spins are caused by the band crossing with the four-qp configurations.

Taking a survey of the band diagrams in Figs. 2–4, we clearly see the evolution of the two-qp and four-qp band

TABLE II. Two-quasiparticle configurations for neutrons and protons.

Neutron	Configuration	Proton	Configuration
$2n_1$	$\nu 1/2[440] \otimes \nu 3/2[431]$	$2p_1$	$\pi 3/2[321] \otimes \pi 5/2[312]$
$2n_2$	$\nu 3/2[431] \otimes \nu 5/2[422]$	$2p_2$	$\pi 1/2[300] \otimes \pi 3/2[321]$
$2n_3$	$\nu 5/2[422] \otimes \nu 7/2[413]$		

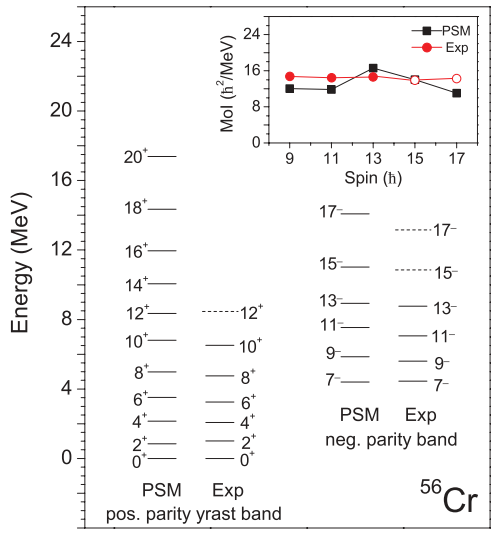

FIG. 5. (Color online) Comparison of calculated energy levels with data [15] for the positive-parity yrast band and the negative-parity band in ^{56}Cr. Dashed lines denote tentatively assigned data. Inset: Comparison of calculated moment of inertia with data for the negative-parity band.

structures along the isotopic chain imposed by shell fillings. With increasing neutron number, the role of the $g_{9/2}$ orbit changes with occupation of different K states because the nucleons that first align their spin vary among the isotopes of interest. For the mass region with less dense single-particle levels, a distinct behavior in observable quantities such as the MoI can be detected in neighboring isotopes.

The current experimental data, however, limit possible comparisons between calculations and experiment for high-spin yrast states and do not allow us to draw strong conclusions about the relevance of the calculated results. This is particularly bothersome because Fig. 1 indicates discrepancies between calculations and experiment at the highest spin states of the experimental bands. However, there is at least one negative-parity band in ^{56}Cr that has been observed [15] up to high spins. This band has a two-qp structure with one qp from the neutron $g_{9/2}$ orbital. In Fig. 5, we compare two rotational bands of ^{56}Cr with data taken from Ref. [15]. These are the lowest positive-parity (yrast) band and the lowest negative-parity band obtained from the calculation. The calculation reproduces nicely the bandhead energy as well as the rotational feature of the negative-parity band. The inset MoI plot in Fig. 5, however, indicates that the calculation exaggerates the proton $f_{7/2}$ alignment at $I = 13$, with a larger peak in MoI than the data show. This suggests that one must be cautious regarding the quantitative details of the prediction in Fig. 1, although we do not expect that small discrepancies would change the alignment picture discussed here.

As the entire discussion in the present work depends on the single-particle states, it is important to comment on the deformed Nilsson scheme employed in the model basis. The Nilsson parameters used for the present discussions were fitted to the stable nuclei a long time ago [23]. It has been shown that the standard Nilsson parameters may need adjustments when they are applied to proton- or neutron-rich regions [24,25]. For neutron-rich nuclei with a considerable neutron excess, use of the standard parameter set needs to be validated. It would not be surprising if the Nilsson parameters used here require a modification. Thus future experiments on high-spin yrast spectra will be compared with the present predictions and serve as a guide for modification of the deformed single-particle scheme.

In conclusion, the present study has highlighted the role of the proton $f_{7/2}$ and neutron $g_{9/2}$ orbits that are involved in the discussion of neutron-rich nuclei. As we have studied in detail, excitation to these orbits leads to pronounced observation effects at high spins, where variations in the MoI are explained in terms of rotation alignment of the high-j particles. As the discussion is based crucially on the deformed single-particle scheme, we emphasize that any future experimental confirmation or refutation of our predictions will be valuable information, which can help to pin down the single-particle structure in this neutron-rich mass region.

Research at Shanghai Jiao Tong University was supported by a Shanghai Pu-Jiang grant, the National Natural Science Foundation of China under Contract No. 10875077, the Doctoral Program of High Education Science Foundation under Grant No. 20090073110061, and the Chinese Major State Basic Research Development Program under Grant No. 2007CB815005.

[1] A. Gade *et al.*, Phys. Rev. C **81**, 051304(R) (2010).
[2] N. Aoi *et al.*, Phys. Rev. Lett. **102**, 012502 (2009).
[3] S. Lunardi *et al.*, Phys. Rev. C **76**, 034303 (2007).
[4] P. Adrich *et al.*, Phys. Rev. C **77**, 054306 (2008).
[5] J. Ljungvall *et al.*, Phys. Rev. C **81**, 061301(R) (2010).
[6] O. Perru *et al.*, Phys. Rev. Lett. **96**, 232501 (2006).
[7] R. Grzywacz *et al.*, Phys. Rev. Lett. **81**, 766 (1998).
[8] M. Hannawald *et al.*, Phys. Rev. Lett. **82**, 1391 (1999).
[9] O. Sorlin *et al.*, Eur. Phys. J. A **16**, 55 (2003).
[10] R. V. F. Janssens, Nature (London) **435**, 897 (2005).
[11] T. R. Rodríguez and J. L. Egido, Phys. Rev. Lett. **99**, 062501 (2007).
[12] F. S. Stephens and R. S. Simon, Nucl. Phys. A **183**, 257 (1972).
[13] Y. Sun *et al.*, Phys. Rev. C **80**, 054306 (2009).
[14] M. Devlin *et al.*, Phys. Rev. C **61**, 017301 (1999).
[15] S. Zhu *et al.*, Phys. Rev. C **74**, 064315 (2006).
[16] O. B. Tarasov *et al.*, Phys. Rev. Lett. **102**, 142501 (2009).
[17] E. Caurier *et al.*, Eur. Phys. J. A **15**, 145 (2002).
[18] M. Honma *et al.*, Eur. Phys. J. A **25**, 499 (2005).
[19] K. Kaneko, Y. Sun, M. Hasegawa, and T. Mizusaki, Phys. Rev. C **78**, 064312 (2008).
[20] L. Gaudefroy *et al.*, Phys. Rev. C **80**, 064313 (2009).
[21] K. Hara and Y. Sun, Int. J. Mod. Phys. E **4**, 637 (1995).
[22] P. A. Dar, R. Devi, S. K. Khosa, and J. A. Sheikh, Phys. Rev. C **75**, 054315 (2007).
[23] T. Bengtsson and I. Ragnarsson, Nucl. Phys. A **436**, 14 (1985).
[24] J. Zhang, Y. Sun, M. Guidry, L. L. Riedinger, and G. A. Lalazissis, Phys. Rev. C **58**, R2663 (1998).
[25] Y. Sun, J. Zhang, M. Guidry, J. Meng, and S. Im, Phys. Rev. C **62**, 021601(R) (2000).